ELSEVIER

Polymer 40 (1999) 315–328

polymer

Undirectional fibre-reinforced polymers: analytical morphology approach and mechanical modelling based on the percolation concept

N.D. Alberola*, G. Merle, K. Benzarti

Laboratoire Matériaux Polymères et Composites, Université de Savoie, Campus Scientifique de Savoie-Technolac, Le Bourget du Lac 73376 Cédex France

Received 18 September 1997; revised 30 January 1998; accepted 18 February 1998

Abstract

An improved self-consistent scheme accounting for the 2D geometric arrangement of fibres within the matrix is proposed to predict the influence of the reinforcement effect of DGEBA/anhydride matrix by unidirectional raw glass fibres or coated fibres with silicone or DGEBA/silane coupling agents. This model is based on both (i) an analytical morphology approach underlying the percolation concept and (ii) the definition of an original 'representative morphological pattern' accounting for local phase inversions owing the heterogeneous morphology of composite materials. It is shown that the nature of fibre sizing can influence the viscoelasticity of composite materials by inducing variations in morphology and then in the mechanical coupling. This could result from the more or less good wettability of fibres by the resin during the process. After removing the reinforcement effect through such a theoretical approach, microstructural changes of the polymer matrix induced by fibres, i.e a decrease in the crosslinking degree of the epoxy network, are quantified but no specific influence of the nature of the interface can be revealed.

Keywords: Unidirectional fibre composite; Percolation; Morphology

1. Introduction

It is well-known that mechanical properties of composite materials are governed by two major factors, (i) the nature of bonds between fillers and polymer matrix and (ii) the reinforcement effect of the polymer by fillers [1–13]. However, there is some difficulty in separating the relative contributions of these key features on the overall mechanical behaviour of the composite materials. For example, changes in the main mechanical relaxation related to the glass transition temperature (T_g) of reinforced polymers could result both from changes in the molecular mobility of polymer matrix induced by interactions at the polymer/filler interfaces and from mechanical coupling effect between phases [5]. Moreover, the magnitude of the reinforcement effect depends not only on properties and relative content of each phase but also on the geometric arrangement of the dispersed phase within the polymer matrix [8,10–14]. In addition, for thermosetting resins reinforced by fillers, changes in the dynamic mechanical properties could also result from changes in the microstructure of the polymer because of secondary reactions leading to variations in the crosslinking degree of the resin [15–18].

Accordingly, to evaluate the relative contribution of microstructural changes including interface effects, it is first required to rigorously predict the reinforcement effect by accounting for the morphology of composite materials. Recently, based on the percolation concept [19,20], we have developed an improved mechanical modelling of the viscoelastic behaviour of particulate composites to describe the enhancement of the reinforcement effect of the polymer due to filler clusters [8].

In this paper, such an approach is extended to quantify the reinforcement effect of an epoxy resin by glass fibres coated with model coupling agents by accounting for the morphology at *meso-* and *micro*scales and its evolution with the fibre content. Thus, this approach was used to predict the following elastic and then viscoelastic moduli of these anisotropic materials, i.e. complex transverse Young's modulus (E_T^*), transverse shear modulus (G_{TT}^*), plane-strain bulk modulus (K_T^*), longitudinal Young's modulus (E_L^*) and longitudinal shear modulus (G_{LT}^*). Only experimental and theoretical data related to the complex transverse Young's modulus of these anisotropic composites are reported in this paper.

Subsequently, this modelling is applied to remove the mechanical coupling effect between phases and then to assess the eventual changes in microstructure of the matrix including 'interface effects'.

* Corresponding author.

0032-3861/98/$ - see front matter
PII: S0032-3861(98)00195-5

2. Experimental

2.1. Materials

2.1.1. Matrix

The epoxy resin and the curing agent used in this study are a diglycidyl ether of Bisphenol-A (DGEBA) and a methyl tetra hydrophtalic anhydride (MTHPA), respectively, provided by the CIBA Company (Switzerland).

2.1.2. Unidirectional glass fibres

Unidirectional glass fibres provided by Vetrotex International (France) show uniform diameter of 17 μm. Volume fractions of glass fibres precisely determined from the residues of burned specimens at 600°C are close to 23 and 48 vol.% for each model composite. Two coating agents were used for surface treatment of glass fibres: (i) a silane/DGEBA coupling agent based on γ-methacryloxypropylmethoxysilane (A1100, Union Carbide) and (ii) an elastomeric adduct based on silicone of low molecular weight. The amounts of silane/DGEBA and silicone coupling agents determined on the filler basis by burning the glass fibres at 600°C for 30 min are 0.6 and 0.2 wt.%, respectively.

2.1.3. Sample preparation

Unreinforced epoxy material was prepared by curing the reactive mixture in a mould for 2 h at 100°C, and post-cured for 2 h and 10 h at 140 and 150°C, respectively. The three following kinds of composite specimens were processed by filament winding: epoxy reinforced by (i) raw glass fibres, (ii) silane/DGEBA-coated glass fibres and (iii) silicone-coated glass fibres. Impregnated rovings were wound on the mould and then unidirectional fibre composites were cured for the same conditions as those used for the non-reinforced material. To remove the adsorbed water and to give the same thermal history at each sample, specimens were annealed at T_g + 20°C for 30 min under vacuum and then cooled at room temperature. Table 1 lists the characteristics of the composites used in this study and gives the effective fibre contents determined from the residues of burned samples. As it is shown, the void content evaluated by density measurements is negligible in all the materials.

2.2. Test procedures

2.2.1. Differential scanning calorimetry (d.s.c.)

D.s.c. measurements were performed using a Perkin Elmer DSC7. The glass transition temperature (T_g) was determined from the change in the heat capacity baseline for a heating rate of 20°C/min.

2.2.2. Dynamic mechanical spectrometry

Dynamic mechanical spectrometry was performed on unreinforced epoxy and composite materials by using a Metravib viscoanalyser. Composite samples were tested in tension—compression transversely to the fibre axis. This set-up provides the real (E'_T) and imaginary (E''_T) parts of the complex transverse Young's modulus and the internal friction tan $\delta_{E_T}(=E''_T/E'_T)$ as functions of temperature (for one or several frequencies) or of frequency (under isothermal conditions). Parallelepipedic specimens ($20 \times 3 \times 3$ mm) were placed in a thermal jacket and temperature scans were carried out by increasing the temperature from 30 to 200°C with a heating rate of about 1°C/min. Spectra were also recorded under isothermal conditions in the *Tg* region for several frequencies over the range from 5 to 30 Hz. Complex Young's modulus (E^*_m) of the unfilled epoxy network was analyzed in the same experimental conditions.

2.2.3. Scanning electron microscopy (s.e.m.) and image analysis

S.e.m. observations were performed on cross-sectional area of carefully polished and metallized samples by using a CAMBRIDGE Instrument StereoScan 120 scanning electron microscope.

S.e.m. micrographs were digitalized by an image analyser constitued by a video camera PULNIX connected to a computer through a CYCLOP 2-1 card (DIGITAL VISION Co.). Images were then processed by means of a software developed by the 'Reconnaissance des Formes et Visions' Laboratory (INSA-Lyon, France).

Table 1
Characteristics of composite materials used in this study

Composite materials	Fibre content (vol.%)	Effective fibre content (vol.%)	Void content (vol.%)
DGEBA/anhydride matrix refinforced by raw glass fibre	20	23	< 1.0
	50	48	< 0.8
DGEBA/anhydride matrix reinforced by silicone-coated glass fibres	20	21	< 1.1
	50	43	< 0.8
DGEBA/andhydride matrix reinforced by silane/DGEBA-coated glass fibers	50	45	< 1.1

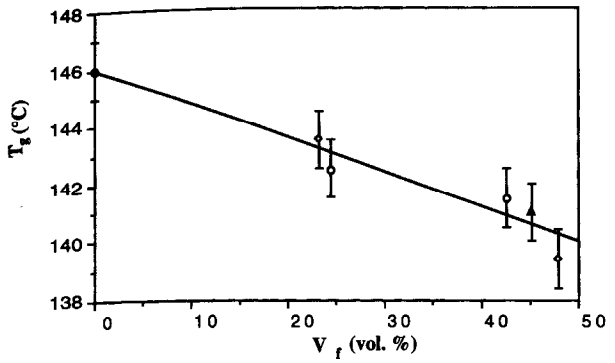

Fig. 1. Evolution of T_g *versus* the fibre content for epoxy matrix reinforced by (◇) raw glass fibres, (○) silicone-coated glass fibres and (▲) DGEBA/silane-coated glass fibres. Data for unreinforced epoxy resin (●).

3. Experimental results

3.1. D.s.c. measurements

Fig. 1 shows the evolution of the glass transition temperature (T_g) versus the volume fraction of glass fibres. With increasing the filler content, T_g of composite materials is linearly shifted towards the lower temperatures, regardless of the nature of the fibre surface treatment. Such a decrease in *Tg* also observed by other authors [15,16] for composite materials based on the same kind of epoxy matrix, i.e. DGEBA/anhydride resin, could result from a decrease in the crosslinking degree of the epoxy network [15–18]. As a matter of fact, water molecules bound to the glass fibre surfaces could induce (i) hydrolysis reactions of the anhydride groups and (ii) secondary reversible condensation/esterification reactions, both resulting in a reduced tightness of the network.

3.2. Dynamic mechanical spectrometry

Fig. 2 shows $E'_{(T)}$ and tan $\delta_{(E_T)}$ spectra recorded at 5 Hz in the temperature range from 100 to 200°C for unreinforced epoxy network and composite materials exhibiting the highest content of glass fibres, i.e. close to 45 vol.%. In Table 2 are reported values of the following viscoelastic characteristics: (i) the temperature location of the main relaxation related to T_g ($T\alpha$), (ii) the height of the tan δ peak (tan δ_{max}) and (iii) the glassy (E'_g) and rubbery ($E\delta_c$) moduli, displayed by all the materials.

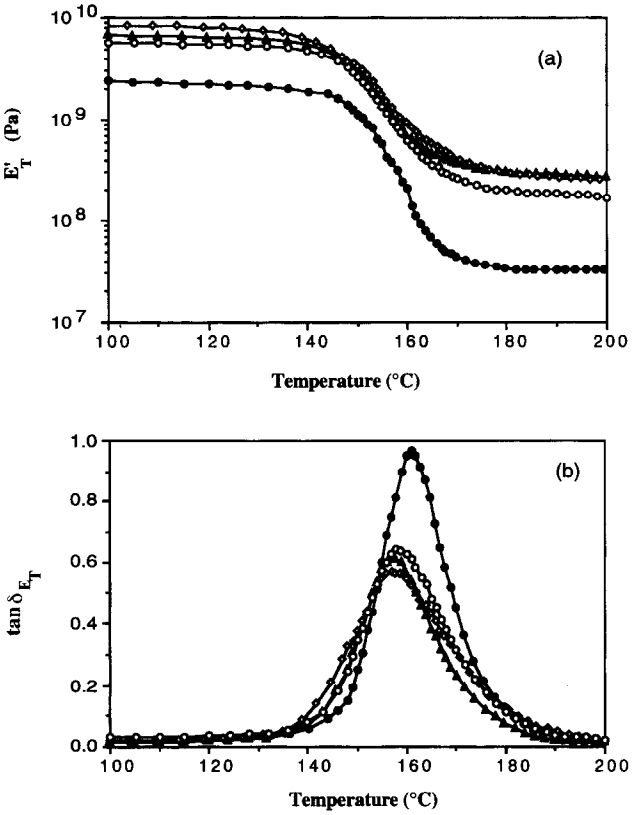

Fig. 2. Experimental variations of E'_T (a) and tan δ_{E_T} (b) *versus* temperature at 5 Hz for composites reinforced by (◇) 48 vol.% of raw glass fibres, (○) 43 vol.% of silicone-coated glass fibres and (▲) 45 vol.% of DGEBA/silane-coated glass fibres. Data for unreinforced epoxy network (●).

The analysis of data leads to the following observations:

1. the main relaxation displayed by composite materials is shifted towards the lower temperatures, regardless of the nature of the interface;
2. both the decrease in the height of the main relaxation and the increase in the moduli displayed by composite materials are mainly governed by the filler content and no significant influence of the fibre sizing can be detected.

Table 2
Characteristic issues from dynamic mechanical analysis at 5 Hz of unreinforced epoxy and composite materials

Materials	Fibre content (vol.%)	$T\alpha$ (°C)	tan δ_{max}	E'_g (GPa)	E'_c (MPa)
Unreinforced epoxy	0	161 ± 1	0.97	2.3 ± 0.4	31 ± 5
Epoxy reinforced by raw glass fibres	23	159 ± 1	0.76	5.2 ± 0.8	94 ± 15
	48	156 ± 1	0.57	9 ± 2	270 ± 40
Epoxy reinforced by silicone-coated glass fibres	43	158 ± 1	0.64	7 ± 2	190 ± 30
Epoxy reinforced by silane/DGEBA-coated glass fibres	45	157 ± 1	0.60	8 ± 2	280 ± 40

Accordingly, modifications of the viscoelasticity of epoxy matrices induced by fibres can be interpreted as follows. The shift of $T\alpha$ towards the lower temperatures displayed by all the composite materials could indicate an increase in the molecular mobility of the polymer matrix near T_g and then a change in the microstructure of the epoxy network induced by fibres. Such an evolution agrees with conclusions derived from d.s.c analysis and no specific influence of the nature of the polymer/fibre interface is detected. The decrease in the damping factor exhibited by composite materials, usually observed, regardless of kind of polymer matrix or the nature of the interface, could mainly result from the reinforcement effect of the epoxy network by fillers. As such, a strong reinforcement effect of the polymer matrix is also observed for low volume fractions of fibres, it could be suggested that composite materials show particular geometric arrangement of fibres within the polymer matrix leading to an enhancement of the mechanical coupling between phases. Morphology analysis is then required to confirm such an hypothesis. Moreover, the increase in the moduli observed for composite materials can be related, to a first approximation, to the reinforcement effect of the polymer matrix by fillers. Then, it is of interest to separate the relative contribution of mechanical coupling effect from that due to microstructural changes of epoxy matrix on the overall viscoleasticity of composites materials. This requires the development of a micromechanical modelling based on a quantitative morphology analysis of composite materials to predict the sole reinforcement effect of the epoxy network by fibres and subsequently to describe the actual viscoelasticity of epoxy matrices.

3.3. S.e.m. observations and image analysis

Because unidirectional composite materials used in this study were processed by filament winding, they exhibit a very heterogeneous morphology for low fibre content, regardless of the nature of the fibre sizing. For example, Fig. 3a shows the 2D geometric arrangement of fibres for composite reinforced by 23 vol.% of raw glass fibres. It can be observed that fibres are packed into bundles embedded within the polymer showing connectivity at the sample scale. Moreover, as shown in Fig. 3b, these *meso*structures are limited on their outers by connected glass fibres. Then, the polymer entrapped within these dense glass fibre zones shows no connectivity with the matrix surrounding the fibre bundles and it can be defined as nonpercolated.

Fig. 4 shows the morphology of composites reinforced by (a) 48 vol.% of raw fibres, (b) 43 vol.% of silicone-coated fibres and (c) 45 vol.% of silane-coated fibres. Some differences in the morphology at *micro*- and *meso*scales can be observed between these composite materials. Thus, the epoxy reinforced by raw glass fibres shows some dense zones of fillers randomly distributed within the polymer matrix but original fibre bundles are no more well-identified (Fig. 4*a*). In contrast, for the composite reinforced by

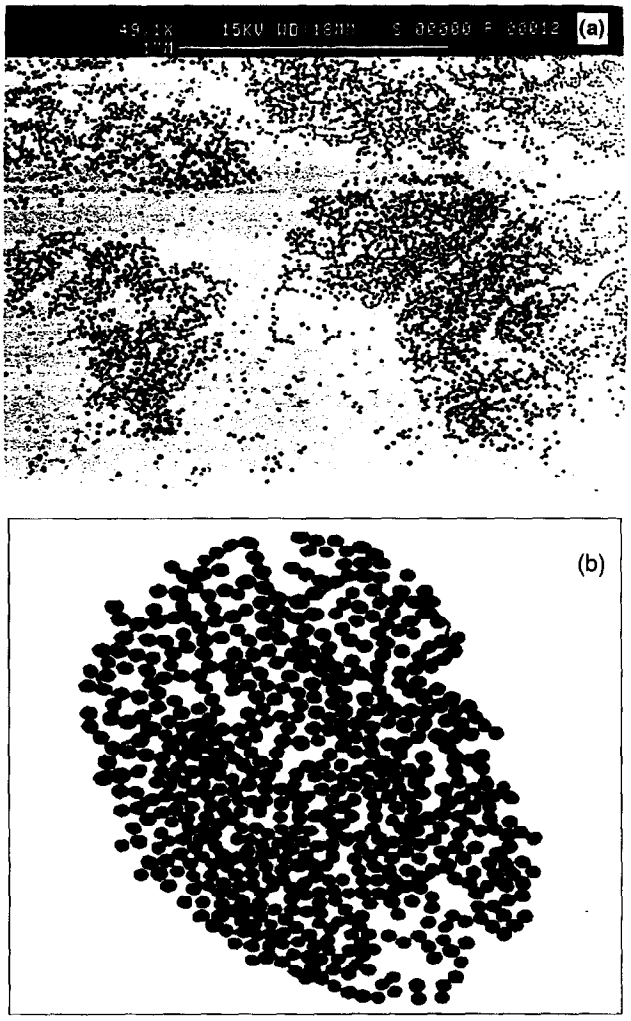

Fig. 3. (a) S.e.m. observations of 2D geometric arrangement of fillers in composite reinforced by 23 vol.% of raw glass fibres. (b) Digital image of a fibre bundle limited by connected glass fibres (——).

silicone-coated glass fibres, mesostructures can still be distinguished. At the microscale, morphology of such composites is also characterized by some variations in the mean fibre spacing. The composite reinforced by high content of silane/DGEBA-coated glass fibres also shows some fibre clusters which are randomly distributed. In addition, mean diameter of these fibre clusters seem to be smaller than that exhibited by the composite reinforced by silicone-coated glass fibres.

Accordingly, for low as for high volume fractions of fibres, composite materials exhibit heterogeneous morphology at *meso*- and *micro*scales characterized by the presence of fibre clusters of which both size and topology seem to be governed by the nature of the filler sizing. Subsequently, this yields to a variable part of the nonpercolated polymer.

Digital image analysis could provide accurate characterization of the 2D geometric arrangement of fibres within the polymer matrix at different scales. Thus, the statistical

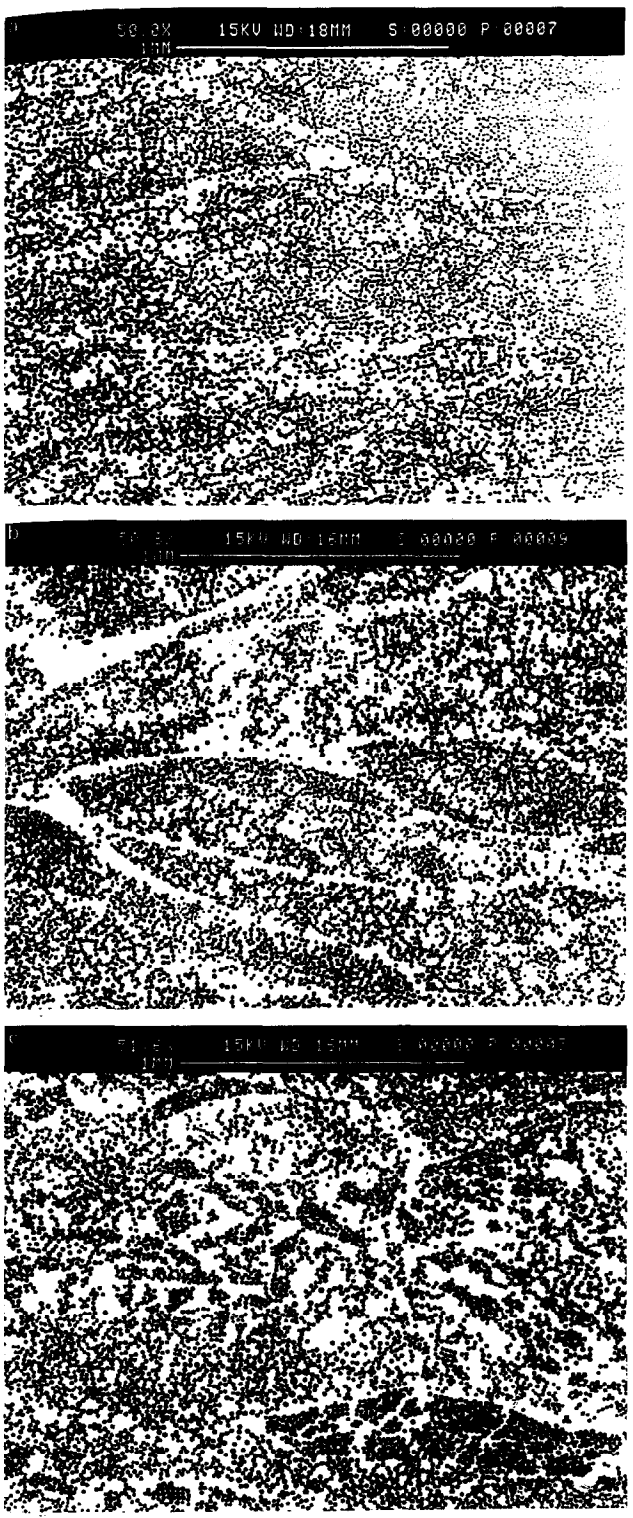

Fig. 4. S.e.m. obsevations of 2D geometric arrangement of fillers in composites showing (a) 48 vol.% of raw glass fibres, (b) 43 vol.% of silicone-coated glass fibres and (c) 45 vol.% of DGEBA/silane-coated glass fibres.

analysis of the nearest-neighbour distance is used to evaluate the uniformity of the local filler distribution [21]. Moreover, the determination of the contents of the percolated and nonpercolated polymer provides information on the mesostructure of such composite materials.

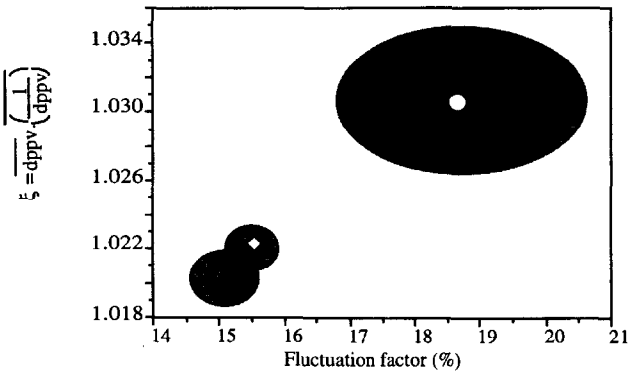

Fig. 5. Variation of the ξ parameter *versus* the fluctuation factor ($\sigma_{dppv}/\overline{dppv}$) for composites reinforced by (◇) 48 vol.% of raw glass fibres, (○) 43 vol.% of silicone-coated glass fibres and (▲) 45 vol.% of DGEBA/silane-coated glass fibres.

From the statistical distribution of the nearest-neighbour distance, the four following parameters are determined: (i) the average fibre spacing, $\overline{dppv}$, (ii) the standard deviation, σ_{dppv}, (iii) the fluctuation factor, $100\cdot(\sigma_{dppv}/\overline{dppv})$ and (iv) the ξ parameter defined by $\xi = \overline{dppv}\cdot\overline{(1/dppv)}$ where $\overline{(1/dppv)}$ is the reciprocal nearest neighboring distance. The fluctuation factor is all the greater as the dispersion quality of fillers is lower. The ξ parameter is equal to 1 for a perfect dispersion of fillers. Higher values of such a parameter reflects the presence of filler strings. Fig. 5 shows the evolution of the ξ parameter *versus* the fluctuation factor for composite materials reinforced by the highest contents of fibres. For each material, reported mean values are calculated from the analysis of six images. The epoxy reinforced by silicone-coated glass fibres is characterized by a high value of the fluctuation factor accompanied by a strong tendancy to fibre cluster formation. This could result from the weak wettability of silicone-coated fibres by the DGEBA/anhydride polymer. In contrast, the composite reinforced by silane-coated glass fibres exhibits a more homogeneous distribution of fibres characterized by a decrease in both the fluctuation factor and the ξ parameter. This could be due to the good miscibility between the coupling agent based on DGEBA prepolymer and the epoxy resin.

The evaluation of the content of nonpercolated polymer is performed by using a simple mathematical morphology analysis [22]. An iterative algorithm of digital image closings and openings allows one to distinguish between percolated and nonpercolated polymer in 2D. The mean data tabulated in Table 3 are from the analysis of six images for each sample. A morphological parameter, χ, accounting for entrapped polymer can be defined as follows:

$$\chi = \frac{V_m - V_{mp}}{V_f} \quad (1)$$

where V_m, V_{mp} and V_f ($= 1 - V_m$) are the volume fractions of the overall polymer, of the percolated matrix and of fibres, respectively.

Table 3
Mean volume fractions and standard deviations of fibre, percolated matrix and nonpercolated polymer determined from image analysis

Materials	Fibre content (vol.%)	Content of percolated polymer (vol.%)	Content of nonpercolated polymer
Epoxy reinforced by raw glass fibres	23 ± 5 48 ± 1	53 ± 8 31 ± 4	23 ± 3 21 ± 3
Epoxy refinforced by silicone-coated glass fibres	43 ± 1	36 ± 4	23 ± 3
Epoxy reinforced by silane/DGEBA-coated glass fibres	45 ± 1	33 ± 3	23 ± 2

For low volume fractions of fillers, the morphological parameter can be related to the average spread of original strands as follows:

$$\chi = \chi_0 = \frac{V_{\text{mbundle}}}{V_f} \tag{2}$$

where V_{mbundle} is the volume fraction of entrapped polymer within the fibre bundles.

Thus, χ_0 value is found to be ~1 for the composite reinforced by 23 vol.% of raw glass fibres and it tends to be decreased for the composite showing the lowest volume fraction of silicone-coated glass fibres. This could result from the poor compatibility between the silicone agent and the epoxy resin which could lead to a reducing in the roving impregnation during the process. By increasing the fibre content, χ is decreased but no specific influence of fibre sizing can be detected.

Thereby, for low as for high volume fractions of fibres, it can be concluded that composite materials exhibit some local phase inversions at the *meso*scale and a part of the polymer matrix can be entrapped within the clusters of fillers.

4. Analytical morphology approach

Based on the percolation theory [19,20], it is now of interest to determine the theoretical evolution of the volume fraction of 'effective' matrix which actually contributes to the viscoelastic behaviour of the composite, i.e. the volume fraction of percolated matrix *versus* the content of polymer by accounting for experimental morphology analysis.

For strand contents ranging from 0 to the percolation threshold of fibre bundles, V_{cbundle}, the volume fraction of percolated matrix, V_{mp}, can be expressed by the following relationship:

$$V_{\text{mp}} = V_{\text{m}} - V_{\text{mbundle}} = V_{\text{m}} + \chi_0(V_{\text{m}} - 1) \tag{3}$$

By increasing the volume fraction of strands from the percolation threshold, V_{cbundle}, of these entities assumed to be disks in 2D, these mesostructures are progressively connected at the sample scale and tend to loose their identities. Then, a progressive evolution of the morphology of the composite occurs from a 'fibre bundle structure' to a 'random fibre structure' (Fig. 3). At V_{cbundle}, the corresponding critical polymer content, V_{cm}, can be expressed by:

$$V_{\text{cm}} = \frac{1 + \xi_0 - V_{\text{cbundle}}}{1 + \chi_0} \tag{4}$$

In 2D, the percolation threshold of disks can theoretically vary from 0.5 (triangular lattice) to 0.7 (hexagonal lattice) [19–23]. Because fibre bundles are randomly distributed within the polymer matrix, we have chosen $V_{\text{cbundle}} = 0.5$ for numerical simulation.

Then, for $V_{\text{m}} \leq V_{\text{cm}}$, the volume fraction of percolated matrix obeys the percolation law. According to the following boundary conditions:

1. at the maximum packing fraction of fibres, V_{fmax}, theoretically calculated and equal to $\pi/\sqrt{3} \approx 0.91$ in 2D, a macroscopic phase inversion occurs and $V_{\text{mp}} = 0$ for $V_{\text{m}} = V_{\text{mmin}}$ with $V_{\text{mmin}} = 1 - V_{\text{fmax}} = 0.09$, and,
2. at the percolation threshold of fibre bundles and then for $V_{\text{m}} = V_{\text{cm}}$, the volume fraction of percolated matrix obeys both Eq. (3) and the percolation law [19,20], the volume fraction of percolated matrix can be expressed by the following relationship:

$$V_{\text{mp}} = V_{\text{m}}\left(1 - \frac{\chi_0(1 - V_{\text{cm}})}{V_{\text{cm}}}\right)\left[\frac{V_{\text{m}} - V_{\text{mmin}}}{V_{\text{cm}} - V_{\text{mmn}}}\right]^{\beta} \tag{5}$$

where, the critical exponent β is 0.14 in 2D lattice [19,20].

Fig. 6 shows the theoretical variations of the volume fraction of percolated matrix *versus* the overall amount of polymer computed for the following values of the morphological parameter, χ_0: (a) 1.2, (b) 1.0 and (c) 0.8. Experimental data from morphology analysis are also shown for comparison. The transition between regions I and II can be related to the beginning of the morphology evolution from a 'fibre bundle structure' towards a 'randomly fibre structure' and can be also expressed by the evolution of $\chi = f(V_{\text{m}})$. Moreover, with increasing χ_0, the analytical approach predicts a weak but significant decrease in the content of percolated matrix which could traduce a better impregnation of strands by the resin leading to an increase in the entrapped polymer within original fibre bundles. Moreover, the decrease in χ_0 yields to a shift of the morphological transition towards the higher contents of fibres (or the lower amounts of polymer). This could

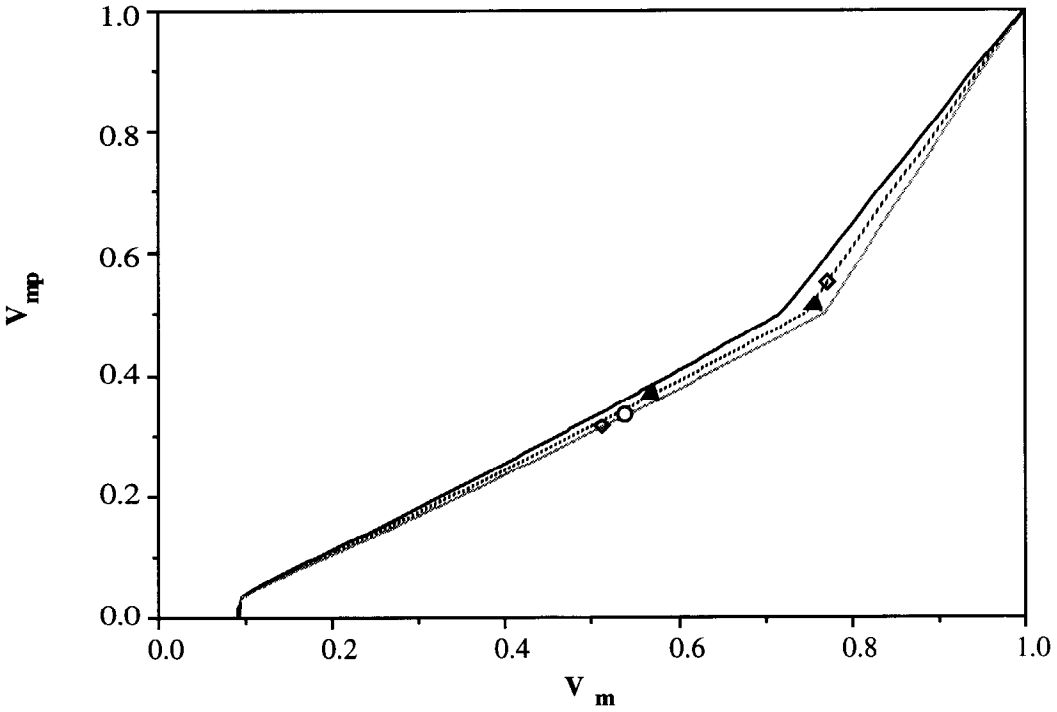

Fig. 6. Theoretical variations of the volume fraction of the percolated polymer, V_{mp}, *versus* the overall amount of polymer, V_m, by taking the morphological parameter χ_0 equal to (bottom line) 1.2, (middle line) 1.0 and (top line) 0.8. Experimental issues from quantative image analysis for composites reinforced by (◇) raw glass fibres, (○) silicone-coated glass fibres and (▲) DGEBA/silane-coated glass fibres.

explain why original fibre bundles remain rather well-defined in composite reinforced by 43 vol.% of silicone-coated glass fibres.

Now, based on such an analytical morphology approach, it is proposed to rigorously predict the reinforcement effect of the epoxy network by glass fibres by accounting for the morphology evolution over a wide range of (i) fibre contents and (ii) temperatures (or frequencies).

5. Modelling of the reinforcement effect

The prediction of the reinforcement effect of composites by a self consistent scheme first requires the definition of a 'representative morphological pattern' (RMP) characteristic of the material morphology and its evolution with increasing the fibre content. Thus, to account for local phase inversions owing to fibre clusters, the 'RMP' consists of a three-layered cylindrical inclusion in which phase 1 constitutes a cylinder of nonpercolated matrix with the radius R_1, phase 2 is the fibre phase limited by the cylinders with the radii R_1 and R_2 and phase 3, the percolated matrix lying outside the fibre shell, is limited by the radii R_2 and R_3 (Fig. 7). Ratios of radii are defined by:

$$\frac{R_2^2}{R_3^2}-\frac{R_1^2}{R_3^2}=1-V_m,\ 1-\frac{R_2^2}{R_3^2}=V_{mp}\ \text{and}\ \frac{R_1^2}{R_3^2}=V_m-V_{mp} \tag{6}$$

where, according to the polymer content, V_m, the volume fraction of percolated matrix, V_{mp}, is given by:

1. Eq. (3) for $V_{cm} \leq V_m < 1$ (region I of Fig. 6); and by
2. Eq. (5) for $V_{mmin} < V_m \leq V_{cm}$ (region II of Fig. 6)

For the maximum packing fraction of fibres, i.e. for $V_m = V_{mmin}$ and $V_{mp} = 0$, the RMP is reduced to a two-layered

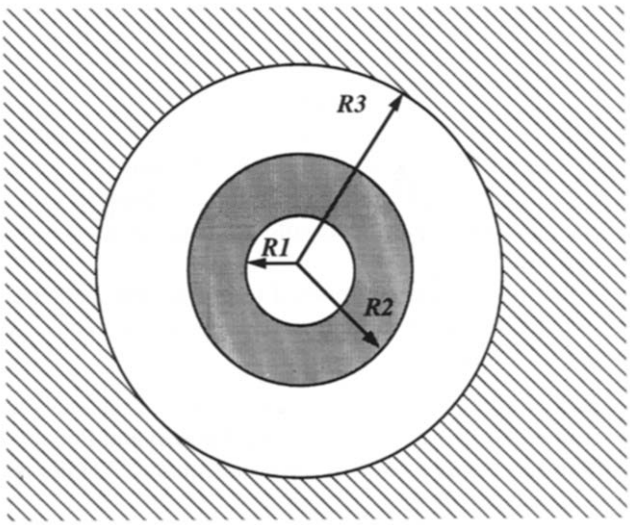

Fig. 7. The 'representative morphological pattern': a three-layered cylindrical inclusion embedded in the homogeneous medium. Phase 1 is the nonpercolated polymer, phase 2 is the filler shell and phase 3 is the percolated matrix.

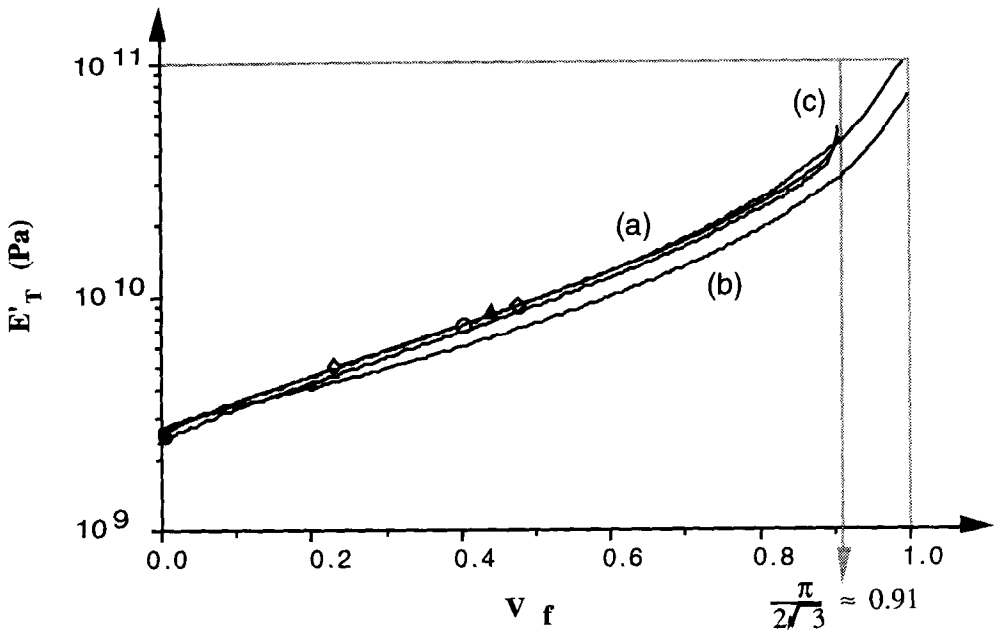

Fig. 8. Plots of theoretical (——) glassy modulus at 30°C, E'_T, (a) from our model by taking χ_0 equal to 1.0 (curves for other χ_0 values are almost superimposed), (b) from Christensen and Lo's model and (c) from Halpin-Tsai's equation. Experimental data for composites reinforced by (◇) raw, (○) silicone-coated and (▲) silane/DGEBA-coated glass fibres.

cylindrical inclusion, i.e. $R_3 = R_2$. Thus, a macroscopic phase inversion occurs and fillers act as the continuous phase. This illustrates the self-consistency of the proposed approach.

Accordingly, elastic properties of the UD fibre composites can be predicted by a (4)-phases self consistent scheme derived from the model developed by Hervé and Zaoui [24] and extended to describe the viscoelastic behaviour by applying the correspondence principle [25]. Thus, the complex transverse Young's modulus of UD fibre composites, E_T^*, can be expressed by the following relationship:

$$E_T^* = \frac{2}{\frac{1}{2K_T^*} + \frac{1}{2G_{TT}^*} + \frac{2\nu_{LT}^{*2}}{E_L^*}} \tag{7}$$

where G_{TT}^* and K_T^* are the complex transverse shear and the plane-strain bulk moduli, respectively. E_L^* and n_{LT}^* are the complex longitudinal Young's modulus and Poisson's ratio, respectively. Detailed calculus of such parameters are given in Appendix A.

In the first step, it is proposed to predict the theoretical reinforcement effect of the epoxy by fibres. Thus, for numerical simulation:

1. glass fibres show an elastic behaviour over the analyzed temperature range. Young's modulus (E_f) and Poisson's ratio (ν_f) of fibres are constant and equal to 73 GPa and 0.2, respectively;
2. viscoelastic properties of the polymer, i.e. both percolated and nonpercolated epoxy, are taken to be identical to those displayed by the unfilled polymer in order to give only evidence for the theoretical influence of the geometric arrangement of fibres on the viscoelasticy of such composites;
3. to account for the glassy-rubbery transition undergone by the polymer through the glass transition, an S-shape variation of the real part of the Poisson's ratio of the matrix is assumed from 0.33 to about 0.5 at $T > T_g$ [8].

The influence of the geometric characteristics of the composite morphology on the viscoelastic properties of the material can be, therefore, assessed by modelling the complex transverse Young's modulus of the composite materials over a wide range of volume fractions of fibres. Fig. 8 shows the evolution of theoretical E'_T at 5 Hz and at 30°C *versus* the fibre content by taking the value of the morphological parameter, χ_0, equal to 1.0 (a). Numerical simulations computed with the other values of the morphological parameter, i.e. 0.8 and 1.2, do not lead to significant changes in the evolution of predicted glassy E'_T *versus* the fibre content and the so-computed curves are almost superimposed. Also in Fig. 8 are shown theoretical issues from Christensen and Lo's self consistent scheme [26] (b) and from the Halpin-Tsai's equation [27] (c), which both do not account for the mesostructure of composite materials. A good agreement can be observed between experimental and theoretical data from both our model and the Halpin-Tsai's equation. As a matter of fact, issues from the improved model and Halpin-Tsai's approach are almost superimposed over the fibre content ranging from 0 to about 0.9. In contrast, Christensen and Lo's model tends to underestimate the reinforcement effect of the polymer matrix by fibres regardless of the fibre content.

To better illustrate the validity of the improved model and then to give evidence of the influence of the morphology on

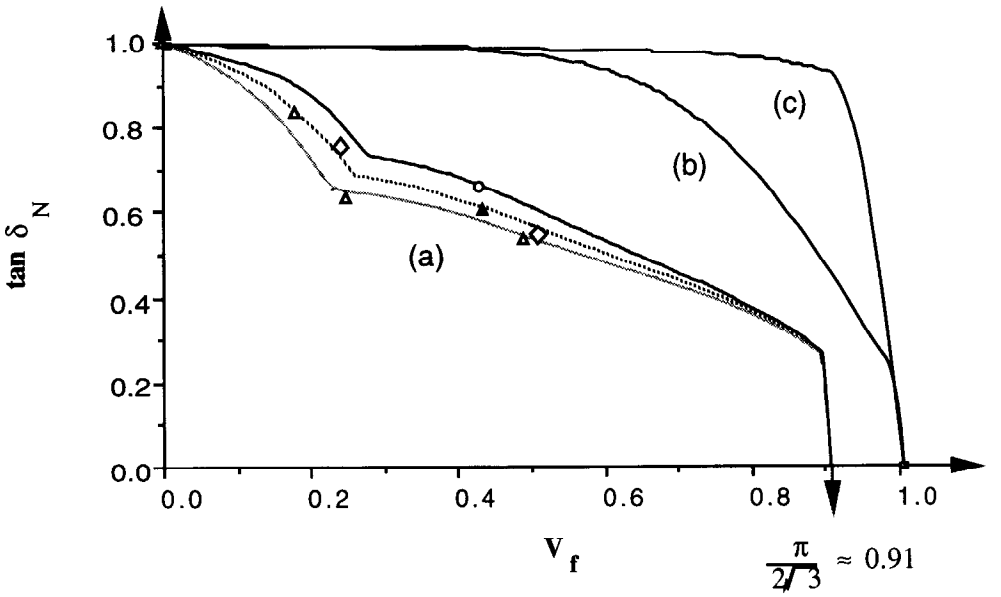

Fig. 9. Plots of theoretical normalized tan δ maximum, tan δ_N, at 5 Hz *versus* the fibre content, (a) from our model by taking χ_0 equal to (bottom line) 1.2, (2nd line up) 1.0 and (3rd line up) 0.8, (b) from Christensen and Lo' self consistent scheme and, (c) from Halpin-Tsai's equation. Experimental data for composites reinforced by (◇) raw, (○) silicone-coated and (▲) silane/DGEBA-coated glass fibres. Experimental data (△) from Lagache's work [28] for silane-coated glass fibres.

micromechanical properties of unidirectional composite materials, it is of interest to compare experimental normalized tan δ_{E_T} maximum (tan δ_N = (tan δ_{E_T}maximum)/(tan δ_{matrix}maximum)) to predict issues from our approach and other models. As a matter of fact, tan δ maximum is a very sensitive parameter to evaluate the magnitude of the mechanical coupling between phases.

Fig. 9*a* shows theoretical variations of tan δ_N *versus* the volume fraction of fibres for the three following values of χ_0: 0.8, 1.0 and 1.2. Also are shown experimental data from Lagache's work [28] dealing with epoxy reinforced by silane-coated glass fibres and issues from the Christensen and Lo model (b) and the Halpin-Tsai equation (c). These models both tend to overestimate the maximum damping value over the analyzed filler content. In contrast, the strong decrease in the damping factor shown by composite materials even for low fibre contents is well predicted by our model, regardless of the nature of the fibre sizing. Moreover, for fibre contents ranging from 0 to about 0.7, tan δ_N is all the greater as χ_0 value is smaller. By taking χ_0 = 0.8, 1.0 and 1.2, predicted tan δ_N are close to experimental data for composites showing silicone-coated, raw and silane/DGEBA-coated glass fibres, respectively. Then, the weak but significant variations in the maximum damping factor observed for composites according to the nature of interface could originate from changes in the morphology which are governed by the compatibility between the coating agent and the polymer matrix.

Now, it is of interest to compare theoretical viscoelastic spectra with experimental ones over the analyzed temperature range. For example, experimental and theoretical values of E'_T and tan δ_{E_T} *versus* the temperature at 5 Hz

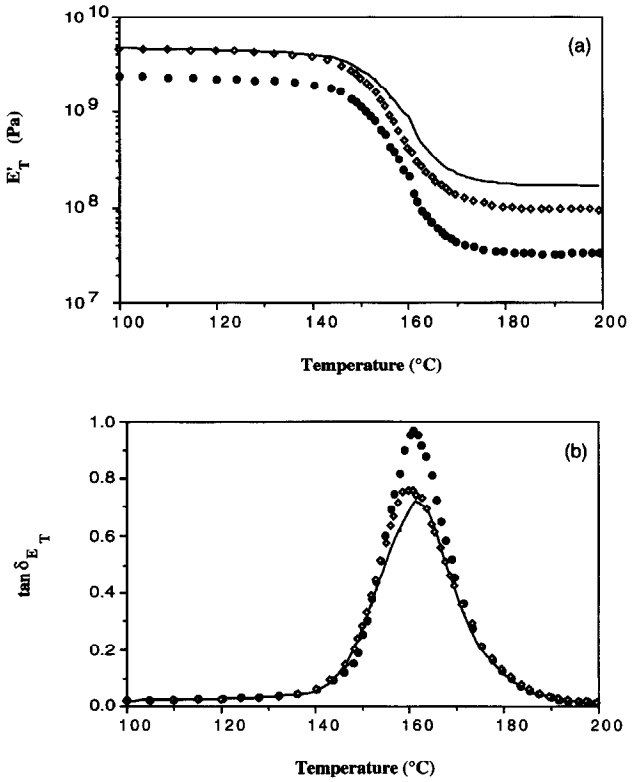

Fig. 10. Theoretical evolutions (——) of E'_T (a) and tan δ_{E_T} (b) *versus* temperature at 5 Hz for the composite reinforced by 23 vol.% of raw glass fibres by taking χ_0 equal to 1.0. Experimental spectra of (□) the composite and of (●) the unreinforced epoxy.

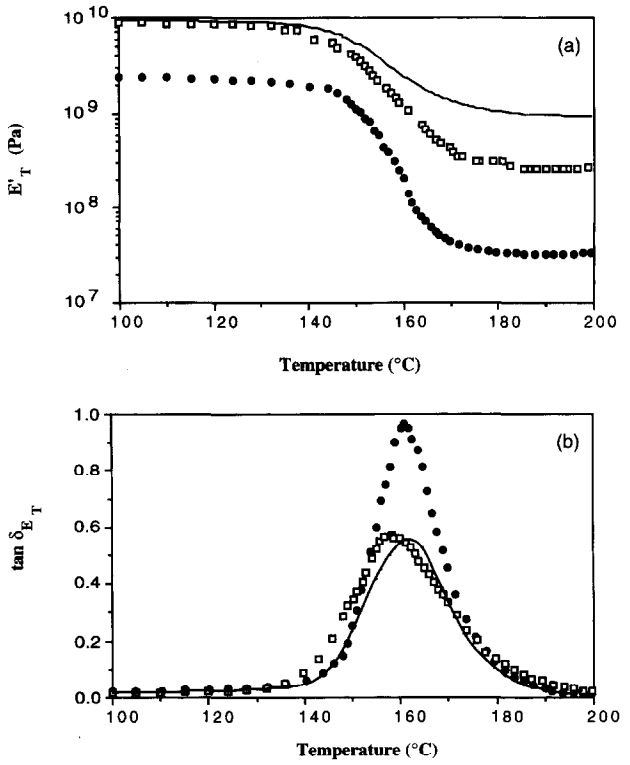

Fig. 11. Theoretical evolutions (——) of E'_T (a) and tan δ_{E_T} (b) *versus* temperature at 5 Hz for the composite reinforced by 48 vol.% of raw glass fibres by taking χ_0 equal to 1.0. Experimental spectra displayed by (□) the composite and by (●) the unreinforced epoxy.

of epoxy polymer reinforced by 23 and 48 vol.% of raw glass fibres are presented in Figs 10 and 11. Theoretical data were computed by taking $\chi_0 = 1.0$.

As it was previously underlined, it can be observed that the model predicts well (i) the real part of the transverse glassy modulus and (ii) the magnitude of the main relaxation of composite materials. Moreover, as it was expected, the model (i) overestimates the rubbery modulus and (ii) does not give evidence for the shift of the relaxation towards the lower temperatures. As a matter of fact, both changes result from a decrease in the crosslinking degree of the epoxy network as it is suggested from d.s.c. analysis. Comparison between experimental and theoretical spectra for all the other composites leads to the same conclusions. Accordingly, the actual viscoelastic behaviour of the epoxy network in composite materials can be derived through the inversion of the modelling in which the viscoelastic properties of the 'modified' matrix (E^*_m) are now the unknown parameters to be assessed. For example, Fig. 12 shows theoretical variations of E'_m and tan δ_{E_m} *versus* the temperature at 5 Hz of the so-called 'modified' DGEBA/anhydride matrices in composites showing 23 and 48 vol.% of raw glass fibres. Experimental data displayed by the unfilled epoxy are also shown for comparison. The glassy moduli of the 'modified' epoxy matrices are very close to that of the unfilled polymer. But, actual epoxy matrices in composites exhibit a significant decrease in the rubbery modulus accompanied by a weak increase in the tan δ maximum. Moreover, such changes in the viscoelasticity of epoxy matrix in composites are found to depend on the amount of fibres, i.e. with increasing the volume fraction of fibres, the rubbery modulus decreases while the damping factor maximum tends to increase. Accordingly, the so-revealed changes in the viscoelasticity of the epoxy matrix induced by fillers are consistent with d.s.c. analysis, i.e. a decrease in the crosslinking degree of the DGEBA/anhydride network, whatever the fibre sizing can be.

6. Microstructural changes of epoxy network induced by fibres

To quantify the changes in the microstructure of epoxy matrix induced by fibres, the main relaxations of the separated matrices are described by means of a physical model for the deformation of amorphous polymer [29] yet applied by the authors to evaluate microstructural changes of the polymer matrix in particulate composites [5]. Through such an approach, the complex Young's modulus of the modified epoxy matrix can be expressed by the following biparabolic equation:

$$E^* = E_r + \frac{E_u - E_r}{1 + H(i\omega\tau_{mr})^{-h} + (i\omega\tau_{mr})^{-k}} \quad (8)$$

where ω is the pulsation, and E_u and E_r are the unrelaxed and the relaxed moduli, respectively. τ_{mr} is the relaxation time. The parameter k ($0 < k < 1$) is consistent with the local motion ability of the chains. Then, k decreases with the material density. The parameter h ($0 < h < 1$) is related to the magnitude of the correlation effects of cooperative molecular motions near T_g. Then, the increase in the number junction points, as for example chemical ties which hinder the molecular mobility at a large scale, results in a decrease of h. H is a function of h, k and E_u.

To determine values of such parameters, E'' is plotted *versus* E' through a computational method developed elsewhere [5], for all the 'modified' matrices. The k and h values are obtained from the slopes of tangents to the 'Cole–Cole' diagrams at lower and higher temperatures, respectively. E_u and E_r values correspond to the intersection points of 'Cole–Cole' diagram with the E' axis at lower and higher temperatures, respectively.

Characteristics determined from the 'Cole–Cole' diagrams and theoretical $T\alpha$ locations for the all polymer matrices within the composite materials are reported in Table 4. Thus, by increasing the fibre content, the main relaxation is shifted towards the lower temperatures and E_r is decreased while h parameter tends to increase. But, no significant changes in k and E_u values are detected. The changes revealed in the microstructure of the polymer matrices agree with the conclusions from the previous analysis. As a matter of fact, the shift of the main relaxation displayed by actual matrices in composites is consistent

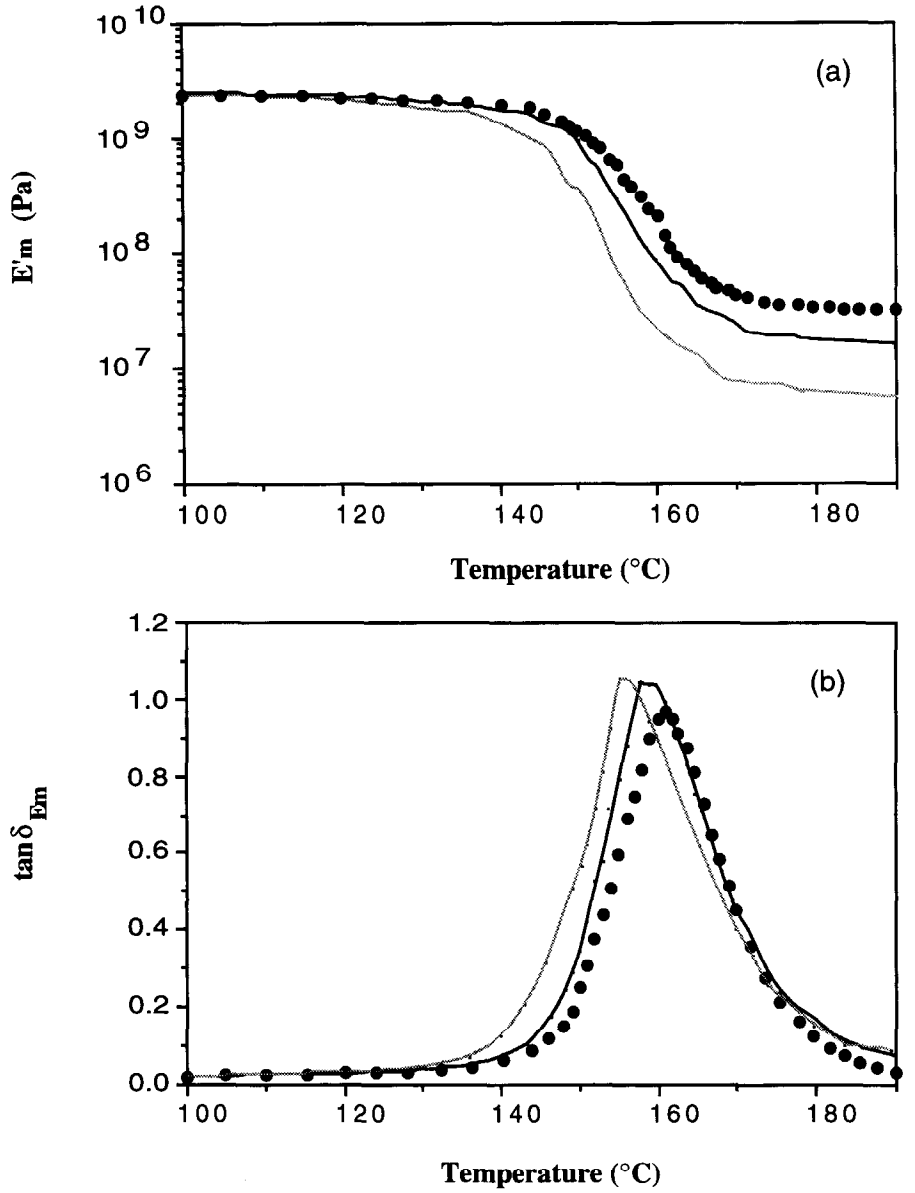

Fig. 12. Plots of E'_m (a) and tan δ_{E_m} (b) *versus* temperature at 5 Hz for actual polymer matrix in composites showing (——) 23 and (——) 48 vol.% of raw glass fibres. Experimental data for the unreinforced epoxy (●).

Table 4
Characteristics values determined for matrices in composite materials. Also given are data for the unreinfored eoxy network

Actual epoxy matrices reinforced by	Fibre content	k	h	tan δ_{max}	$T\alpha$ (°C)	E'_u (GPa)	E'_r (MPa)
raw glass fibres	23	0.26	0.74	1.04	159 ± 1	2.2 ± 0.4	19 ± 4
	48	0.27	0.77	1.08	156 ± 1	2.0 ± 0.4	8 ± 1
silicone-coated glass fibres	43	0.26	0.76	1.06	157 ± 1	1.8 ± 0.3	7 ± 1
DGEBA/silane-coated glass fibres	45	0.27	0.77	1.06	158 ± 1	1.7 ± 0.3	7 ± 1
Unreinforced epoxy	0	0.24	0.73	0.97	161 ± 1	2.3 ± 0.4	31 ± 5

with an improvement in the molecular motion ability of the epoxy network. The increase in h accompanied by a decrease in E_r for actual matrices could produce an increase in the mean molecular weight between two successive junction points leading to a decrease in both the rubbery modulus and the magnitude of correlation effects in cooperative molecular motions. Moreover, the magnitude of such microstructural changes of the polymer seems to only depend on the filler content and not the nature of the fibre sizing. Accordingly, for the composite reinforced by silane-coated fibres, it could be concluded that (i) interactions at the polymer/coated fibres interface do not significantly reduce the molecular motion ability at a large scale or (ii) the induced effects by interactions at the polymer/fibres interface could be strongly counterbalanced by the strong decrease in the tightness of the epoxy network.

7. Conclusion

A theoretical approach based on the percolation concept is proposed to predict the reinforcement effect of DGEBA/anhydride network by undirectional raw or coated glass fibres over a wide range of (i) fillers and (ii) temperatures (or frequencies) and, subsequently, to quantify the microstructural changes of the polymer matrix induced by fibres.

Dynamic mechanical spectrometry analysis performed on composite materials in tension-compression mode transversely to the fibre axis gives evidence for both a strong decrease in the damping factor and an increase in the real part of the complex transverse Young's modulus accompanied by a shift of the main relaxation towards the lower temperatures with increasing the filler content. In agreement with d.s.c. analysis near T_g, the $T\alpha$ shift could result from an increase in the molecular motion ability due to secondary reactions between epoxy resin and water molecules bound to the fillers. The strong decrease in the damping factor even observed for the lowest fibre contents is attributed to enhanced mechanical coupling effects between phases because of heterogeneous morphology of composite materials. Such an hypothesis is confirmed by 2D image analysis showing more or less homogeneous distribution of fibres within the polymer matrix according to the fibre sizing and content. Thus, epoxy reinforced by the lowest fibre contents exhibit *meso*structures constitued of fibre bundles within which a part of the polymer is entrapped. For the composites reinforced by the highest filler contents, some fibre clusters are randomly distributed and also result in local phase inversions. Significant changes in the 2D fibre distribution of fibres can be detected according to the nature of the sizing. Thus, the composite reinforced by fibres coated with the silane/DGEBA coupling agent shows the more homogeneous 2D arrangement of fillers. To assess the 'effective' volume fraction of polymer which really contributes to the viscoelasticity of composites, i.e. the content of percolated polymer, over a wide range of fibre content, an analytical morphology approach is developed based on the percolation concept. A good agreement is found between theory and experimental data from the quantitative image analysis. An improved self-consistent scheme is proposed to predict the reinforcement effect of the epoxy matrix by fibres accounting for the spatial distribution of fibres and its evolution with increasing the filler content. It is based on the definition of one 'representative morphological pattern' constituted of a three-layered cylindrical inclusion, i.e. the nonpercolated polymer entrapped within dense zones of fibres embedded in the percolated matrix. Such a model predicts well the strong reinforcement effect of the polymer matrix by fibres, i.e. both the increase in the modulus and the decrease in the damping factor displayed by composite materials, for high as for low volume fractions of fillers. Subsequently, to assess the actual viscoelastic behaviour of polymer matrix in composites, the model is applied to remove the reinforcement effect induced by fillers. Quantitative microstructural analysis of separated matrices by a physical approach gives evidence for an increase in the molecular mobility consistent with a decrease in the crosslinking degree of the epoxy network in composites. The magnitude of such a microstructural change of the epoxy matrix depends on the fibre content and no specific influence of the nature of the fibre sizing has been detected.

Appendix

The complex transverse Young's modulus of UD fibre composites, E_T^*, is given by the following relationship:

$$E_T^* = \frac{2}{\frac{2}{2K_T^*} + \frac{1}{2G_{TT}^*} + \frac{2\nu_{LT}^{*2}}{E_L^*}}$$

Accordingly, the determination of the following elastic and then viscoelastic parameters of unidirectional fibre composites are required: G_{TT}: the transverse shear modulus; K_T: the plane-strain bulk modulus; E_L: the longitudinal Young's modulus; G_{LT}: the longitudinal shear modulus; and ν_{LT}: the longitudinal Poisson's ratio.

The transverse shear modulus, G_{TT}, is predicted by a (4)-phase self-consistent scheme derived from Herve and Zaoui's model [24]. The other mechanical parameters, K_T, E_L, G_{LT} and ν_{LT} are derived from the composite cylinder assemblage (CCA) approach developed by Hashin and Rosen [30] and generalised to the prediction of the elastic constants of an n-layered cylindrical inclusion [24].

Thus, the final solution for the complex shear modulus, G_{TT}^*, is given by the solution of the following quadratic equation:

$$A\left(\frac{G_{TT^*}}{G_{mp}^*}\right)^2 + 2B\left(\frac{G_{TT}^*}{G_{mp}^*}\right) + C = 0$$

where subscript mp refers to the percolated matrix and

constants A, B and C are defined by the following relationships:

$$A=(3-4\nu_n)(Z_{41}+Z_{32})-(3-4\nu_n)^2Z_{13}+Z_{42}+Z_{43}-3Z_{13}-3Z_{12}$$

$$B=(2\nu_n-1)(Z_{41}+Z_{32})-(3-4\nu_n)Z_{13}-(Z_{42}+Z_{43}-3Z_{13}-3Z_{12})$$

$$C=Z_{42}+Z_{43}-3Z_{13}-3Z_{12}-(Z_{41}+Z_{32}+Z_{13})$$

and

$$Z_{\alpha\beta}=Q_{\alpha4}^{(n-1)}\cdot Q_{\beta1}^{(n-1)}-Q_{\beta4}^{(n-1)}\cdot Q_{\alpha1}^{(n-1)}$$

$$Q^{(n)}=\prod_{i\ l}^{n}N^{(i)}$$

with

$$N^i=\frac{1}{4(1-\nu_{i+1})}\begin{pmatrix}\frac{a_i}{q_i^2} & \frac{1}{q_i^2}(1-\rho_i) & \frac{1}{q_i^2}(1-\rho_i) & 0\\ 2\cdot q_i^4 b_i & q_i^4 c_i & 2\cdot q_i^4 d_i & q_i^4\cdot(\rho_i-1)\\ -3\cdot q_i^2\cdot(1-\rho_i) & 0 & q_i^2 a_i & q_i^2\cdot(1-\rho_i)\\ -6\cdot d_i & 3\cdot(1-\rho_i) & 2\cdot b_i & c_i\end{pmatrix}$$

$$a_i=\rho_i+(3-4\nu_i) \qquad b_i=(3-2\nu_i)+\rho_i.(2\nu_{i+1}-3)$$
$$c_i=1+\rho_i.(3-4\nu_{i+1}) \quad d_i=2\nu_i-1+\rho_i\cdot(1-2\nu_{i+1})$$

$$\rho_i=\frac{G_{TT}^{(i)}}{G_{TT}^{(i+1)}} \text{ and } q_i=\frac{R_i}{R_{i+1}} \text{ with } i\in[1,n-1] \text{ and } q_n=1$$

where α and $\beta\in[1,4]$.

The mechanical parameters K_T, E_L, G_{LT} and n_{LT} are determined through a recursive algorithm. Then, it yields to:

$$K_T^{HR(n)}=\frac{K_T^{(n)}(K_T^{(HR(n-1)}+G_{LT}^{(n)})\cdot(R_n^2-R_{n-1}^2)+K_T^{HR(n-1)}(K_T^{(n)}+G_{LT}^{(n)})\cdot R_{n-1}^2}{(K_T^{HR(n-1)}+G_{LT}^{(n)})\cdot(R^2-R_{-1}^2)+(K_T^{(n)}+G_{LT}^{(n)})\cdot R_{-1}^2}$$

$$\frac{G_{LT}^{HR(n)}}{G_{LT}^{(n)}}=\frac{G_{LT}^{(n)}(R_n^2-R_{n-1}^2)+G_{LT}^{HR(n-1)}(R_{n-1}^2+R_n^2)}{G_{LT}^{(n)}(R_{-1}^2-R^2)+G_{LT}^{HR(n-1)}(R^2-R_{-1}^2)}$$

$$\nu_{LT}^{HR(n)}=\nu_{LT}^{HR(n-1)}\cdot R_{n-1}^2+\nu_{LT}^{(n)}\cdot(R_n^2-R_{n-1}^2)+\frac{R_{n-1}^2(R_n^2-R_{n-1}^2)\cdot(\nu_{LT}^{HR(n-1)}-\nu_{LT}^{(n)})\cdot\left(\frac{1}{K_T^{(n)}}-\frac{1}{K_T^{HR(n-1)}}\right)}{\frac{R_{n-1}^2}{K_T^{(n)}}+\frac{1}{G_{LT}^{(n)}}+\frac{(R_n^2-R_{n-1}^2)}{K_T^{HR(n-1)}}}$$

$$E_L^{HR(n)}=E_L^{HR(n-1)}\cdot R_{n-1}^2+E_L^{(n)}\cdot(R_n^2-R_{n-1}^2)+\frac{4R_{n-1}^2(R_n^2-R_{n-1}^2)\cdot(\nu_{LT}^{HR(n-1)}-\nu_{LT}^{(n)^2})}{\frac{R_{n-1}^2}{K_T^{(n)}}+\frac{1}{G_{LT}^{(n)}}+\frac{(R_n^2-R_{n-1}^2)}{K_T^{HR(n-1)}}}$$

where the exponent HR and subscript n refer to the superimposed bounds of Hashin and Rosen and to the different layers of the composite cylinder, respectively. Effective moduli of the n-layered composite cylinder are equivalent to the Hashin-Rosen bounds: $K_T = K_T^{HR(n)}$, $G_{LT} = G_{LT}^{HR(n)}$, etc. Finally, complex moduli are determined by applying the correspondence principle.

References

[1] Lipatov YS. Adv Polym Sci 1977;22:1.
[2] Plueddemann E. In: Silane coupling agents. New York: Plenum Press, 1982.
[3] Eklind H, Maurer FH. J Polymer 1996;27:2641.
[4] Theocaris PS. In: The mesophase concept in composites. Berlin: Springer Verlag, 1987.
[5] Bergeret A, Alberola N. Polymer 1996;37:2759.
[6] Chauchard J, Chabert B, Jeanne P, Nemoz G. Angew Makromol Chem 1987;154:23.
[7] Lewis TB, Nielsen LE. J Appl Polym Sci 1970;14:1449.
[8] Alberola ND, Mele P. Polym Compos 1996;17:751.
[9] Reed KD. Polym Compos 1980;1:172.
[10] Pigott MR. Compos Sci Technol 1995;35:201.
[11] Yugartis SW. Compos Sci Technol 1995;53:145.
[12] Paluch B. J Compos Mat 1996;30:454.
[13] Hiemstra DL. J Compos Mat 1993;27:1030.
[14] Gao Z, Reifsnider KL, Carman G. J Compos Mat 1992;26:1678.
[15] Lacrampe V. Thesis, Lyon, 1992.
[16] Garton A, Stevenson WTK. J Polym Sci Part A 1988;26:541.
[17] Selliti C, Koenig JL, Ishida H J Polym Sci Part B 1990;28:1121.
[18] Garton A. J Polym Sci Part A 1984;22:1495.
[19] de Gennes PG. In: Scaling concepts in Polymer Physics. Ithaca, NY: Cornell University Press, 1979.
[20] Stauffer D. In: Introduction to percolation theory. London: Taylor and Francis, 1985.
[21] Wimolkiatisak AS, Bell JP, Scola DA, Chang J. Polym Compos 1990;11:274.
[22] Coster CJL. In: Précis d'analyse d'images. Washington: Presses du CNRS, 1989.
[23] Galam S, Mauser A. Physica A 1994;205:502.
[24] Herve E, Zaoui A. Int J Engng Sci 1995;33:1419.
[25] Dickie RA. J Appl Polym Sci 1973;17:65.
[26] Christensen RM, Lo KH. J Mech Phys of Solids 1986;34:639.
[27] Tsai SW, Pagano NJ. In: Composite material workshop. New York: Technomic Publishing Co., 1968.
[28] Lagache M., Thesis, Grenoble, 1993.
[29] Perez J. In: Physique et mécanique des polymères amorphes. Paris: Lavoisier, 1992.
[30] Hashin Z, Rosen WB. J Appl Mech 1964;31:223.